

DMD # 68866

**Biotransformation of Daclatasvir *in Vitro* and in Nonclinical Species: Formation of the Main Metabolite by Pyrrolidine  $\delta$ -Oxidation and Rearrangement**

Wenying Li, Weiping Zhao, Xiaohong Liu, Xiaohua Huang, Omar D. Lopez, John E. Leet, R. Marcus Fancher, Van Nguyen, Jason Goodrich, John Easter, Yang Hong, Janet Caceres-Cortes, Shu Y. Chang, Li Ma, Makonen Belema, Lawrence G. Hamann, Min Gao, Mingshe Zhu, Yue-Zhong Shu, W. Griffith Humphreys, and Benjamin M. Johnson

*Departments of Pharmaceutical Candidate Optimization (W.L., W.Z., X.L., X.H., R.M.F., J.C.-C., S.Y.C., L.M., M.Z., Y.-Z.S., W.G.H., B.M.J.); Synthesis and Analysis Technology Team (J.E.L.); Virology (M.G.) and Chemistry (O.D.L., V.N., J.G., J.E., Y.H., M.B., L.G.H.); Bristol-Myers Squibb Company, Wallingford, Connecticut*

DMD # 68866

**Running title:** Biotransformation of daclatasvir

**Address correspondence to:** Dr. Benjamin M. Johnson, Pharmaceutical Candidate Optimization, Bristol-Myers Squibb Company, 5 Research Parkway, Wallingford, CT 06492. email: [benjamin.m.johnson@bms.com](mailto:benjamin.m.johnson@bms.com).

**Number of text pages:** 53

**Number of tables:** 6

**Number of figures:** 6

**Number of references:** 37

**Number of words in the *Abstract*:** 198

**Number of words in the *Introduction*:** 671

**Number of words in the *Discussion*:** 1482

**Nonstandard abbreviations:** 1D, one-dimensional; 2D, two-dimensional; BDC, bile-duct cannulated; CID, collision-induced dissociation; CV, collision voltage; DP, declustering potential; FID, free induction decay; GSH, glutathione; HCV, hepatitis C virus; HPLC, high-performance liquid chromatography; INF- $\alpha$ , interferon- $\alpha$ ; LC-MS<sup>n</sup>, liquid chromatography-tandem mass spectrometry;  $m/z$ , mass-to-charge ratio; MS, mass spectrometry; NADPH, nicotinamide adenine dinucleotide phosphate (reduced form); NMR, nuclear magnetic resonance; NOE, nuclear Overhauser enhancement; NS5A, nonstructural protein 5A; PEG-INF- $\alpha$ , pegylated interferon- $\alpha$ ; RNA, ribonucleic acid; TRA, total radioactivity analysis; VAP, vascular access port

DMD # 68866

## Abstract

Daclatasvir is a first-in-class, potent and selective inhibitor of the hepatitis C virus nonstructural protein 5A replication complex. In support of nonclinical studies during discovery and exploratory development, liquid chromatography–tandem mass spectrometry and NMR were used in connection with synthetic and radiosynthetic approaches to investigate the biotransformation of daclatasvir *in vitro* and in the cynomolgus monkey, dog, mouse, and rat. The results of these studies indicated that disposition of daclatasvir was accomplished mainly by release of unchanged daclatasvir into bile and feces, and, secondarily, by oxidative metabolism. Cytochromes P450 were the main enzymes involved in the metabolism of daclatasvir. Oxidative pathways included  $\delta$ -oxidation of the pyrrolidine moiety, resulting in ring opening to an aminoaldehyde intermediate followed by an intramolecular reaction between the aldehyde and the proximal imidazole nitrogen atom. Despite robust formation of the resulting metabolite in multiple systems, rates of covalent binding to protein associated with metabolism of daclatasvir were modest (55.2 – 67.8 pmol/mg/h) in NADPH-supplemented liver microsomes (human, monkey, rat) suggesting that intramolecular rearrangement was favored over intermolecular binding in the formation of this metabolite. This biotransformation profile supported the continued development of daclatasvir, which is now marketed for the treatment of chronic HCV infection.

DMD # 68866

## Introduction

Hepatitis C virus (HCV) infection is a global health problem that affects an estimated 130 – 170 million people, representing 2.2 – 3.0% of the world's population (Lavanchy, 2009). The rise of HCV infection to this level of prevalence occurred in the 20th century as a result of person-to-person transmission via parenteral exposure to contaminated blood and medical equipment. Developed countries in North America and Europe have maintained controls since the 1980s that have limited the transmission of HCV during blood transfusions. However, medically related modes of transmission have been a problem in developing countries and have contributed to even higher infection rates in Africa, Southeastern Europe and the Far East. Chronic HCV infections may progress to cirrhosis, hepatocellular carcinoma and/or death, with mortality rates differing among industrialized and developing countries (The Global Burden of Hepatitis C Working Group, 2004).

In the past several years, new options to treat chronic HCV infection have emerged that are replacing the need for therapies based on pegylated interferon- $\alpha$  (PEG-IFN- $\alpha$ ), which are accompanied by unwanted side effects (Rodriguez-Torres *et al.*, 2013). For example, insights into the workings of the HCV replication complex have resulted in direct-acting antivirals against the multiple viral targets. For example, the HCV NS3 protease is one such target that has been the subject of drug discovery efforts (McPhee *et al.*, 2012). New medicines targeting the HCV NS5B polymerase have also been developed, including nucleotide-based inhibitors such as sofosbuvir (Sofia *et al.*, 2010) and non-nucleotide analogs such as dasabuvir that target one of several allosteric sites on the NS5B protein (Lesburg *et al.*, 1999; Bressanelli *et al.*, 1999). Combinations of such

DMD # 68866

medicines have been the subject of clinical studies to determine which combinations are most effective against the different genotypes of HCV, and which might be appropriate for use in patient populations that are difficult to treat. Inhibitors of the non-structural protein 5A (NS5A) represent another important class of direct-acting antivirals that is emerging as a key option in the treatment of such patients (Piroth *et al.*, 2015). While the functionality of NS5A is not fully understood, it is clearly an important component of the HCV RNA replicase complex (Blight *et al.*, 2000). Subgenomic, non-infectious replicon systems enabling the study of this complex in a cellular environment have been developed (Lohmann *et al.*, 1999). NS5A has been characterized as a protein with three discrete structural domains and an amphipathic  $\alpha$ -helix that tethers the protein to the membrane bilayer (Penin *et al.*, 2004). Of these domains, domain I is the best characterized and appears to be the most directly involved in RNA replication. This domain includes a zinc-binding motif that must be coordinated to a zinc atom for RNA replication to occur, and a basic groove – possibly for RNA binding (Tellinghuisen *et al.*, 2004). Crystal structures of this domain have been reported, providing complementary information on its structure (Tellinghuisen *et al.*, 2005; Love *et al.*, 2009; Lambert *et al.*, 2014). It has also been postulated that a higher order of NS5A structure exists, explaining both the exquisite potency of NS5A inhibitors and resensitization of resistant NS5A variants by NS5A synergists (Sun *et al.*, 2015). As a result of its demonstrated critical role in HCV replication, NS5A represents an attractive target for anti-HCV therapy.

Daclatasvir (dimethyl (2*S*,2'*S*)-1,1'-((2*S*,2'*S*)-2,2'-(4,4'-(biphenyl-4,4'-diyl)bis(1*H*-imidazole-4,2-diyl))bis(pyrrolidine-2,1-diyl))bis(3-methyl-1-oxobutane-2,1-diyl)dicarbamate; Fig. 1) is a first-in-class, selective inhibitor of the NS5A replication

DMD # 68866

complex, which evolved from a series of dimeric compounds possessing  $C_2$  symmetry (Belema *et al.*, 2014). It is among the most potent anti-HCV drugs reported thus far, with  $EC_{50}$ s against the wild-type 1a and 1b replicons of 50 pM and 9 pM, respectively (Gao *et al.*, 2010). Combinations of direct-acting antivirals including daclatasvir have demonstrated high cure rates in the clinic, even among difficult-to-treat populations including those infected with genotype 3, patients with cirrhosis or fibrosis, previous non-responders to IFN/ribavirin-based regimens and patients coinfecting with HIV (Nelson *et al.*, 2015; Lok *et al.*, 2012; Chayama *et al.*, 2012; Wyles *et al.*, 2015). Here we report the preclinical biotransformation of daclatasvir, including a full structural characterization of key metabolites.

DMD # 68866

## Materials and Methods

**Substances and Enzymes** Daclatasvir (BMS-790052; **1**), [<sup>3</sup>H]-daclatasvir {[<sup>3</sup>H]-**1**}, [<sup>14</sup>C]-daclatasvir {[<sup>14</sup>C]-**1**} (Easter *et al.*, submitted), and compounds **2** (methyl ((1*S*)-1-(((2*S*)-2-(4-(4'-(2-((2*S*)-1-((2*S*,3*R*)-4-hydroxy-2-((methoxycarbonyl)amino)-3-methylbutanoyl)-2-pyrrolidinyl)-1*H*-imidazol-4-yl)-4-biphenyl)-1*H*-imidazol-2-yl)-1-pyrrolidinyl)carbonyl)-2-methylpropyl)carbamate), **3** (methyl ((1*S*)-1-(((8*S*)-5-hydroxy-2-(4'-(2-((2*S*)-1-((2*S*)-2-((methoxycarbonyl)amino)-3-methylbutanoyl)-2-pyrrolidinyl)-1*H*-imidazol-4-yl)-4-biphenyl)-5,6,7,8-tetrahydroimidazo[1,2-*a*]pyridin-8-yl)carbonyl)-2-methylpropyl)carbamate), **4** (methyl (*S*)-1-(((*S*)-2-(5-(4'-(2-((*S*)-1-((*S*)-2-amino-3-methylbutanoyl)pyrrolidin-2-yl)-1*H*-imidazol-5-yl)biphenyl-4-yl)-1*H*-imidazol-2-yl)pyrrolidin-1-yl)-3-methyl-1-oxobutan-2-yl)carbamate), **6** (two diastereomers: methyl *N*-[1-(2-{5-[4-(4-{2-[(2*S*,4*S*)-4-hydroxy-1-[(2*S*)-2-[(methoxycarbonyl)amino]-3-methylbutanoyl]pyrrolidin-2-yl]-1*H*-imidazol-5-yl}phenyl)phenyl]-1*H*-imidazol-2-yl}pyrrolidin-1-yl)-3-methyl-1-oxobutan-2-yl]carbamate and methyl *N*-[1-(2-{5-[4-(4-{2-[(2*S*,4*R*)-4-hydroxy-1-[(2*S*)-2-[(methoxycarbonyl)amino]-3-methylbutanoyl]pyrrolidin-2-yl]-1*H*-imidazol-5-yl}phenyl)phenyl]-1*H*-imidazol-2-yl}pyrrolidin-1-yl)-3-methyl-1-oxobutan-2-yl]carbamate), **7** (two diastereomers: methyl *N*-[(2*S*)-1-[(2*R*,3*S*)-3-hydroxy-2-{4-[4-(4-{2-[(2*S*)-1-[(2*S*)-2-[(methoxycarbonyl)amino]-3-methylbutanoyl]pyrrolidin-2-yl]-1*H*-imidazol-4-yl}phenyl)phenyl]-1*H*-imidazol-2-yl}pyrrolidin-1-yl)-3-methyl-1-oxobutan-2-yl]carbamate and methyl *N*-[(2*S*)-1-[(2*R*,3*R*)-3-hydroxy-2-{4-[4-(4-{2-[(2*S*)-1-[(2*S*)-2-[(methoxycarbonyl)amino]-3-methylbutanoyl]pyrrolidin-2-yl]-1*H*-imidazol-4-yl}phenyl)phenyl]-1*H*-imidazol-2-yl}pyrrolidin-1-yl)-3-methyl-1-oxobutan-2-yl]carbamate), and **8** (2-(4'-(2-((*S*)-1-

DMD # 68866

((methoxycarbonyl)-*L*-valyl)pyrrolidin-2-yl)-1*H*-imidazol-5-yl)-[1,1'-biphenyl]-4-yl)-2-oxoacetic acid) were synthesized chemically at Bristol-Myers Squibb Co. (Wallingford, CT). The remaining metabolites **5**, **9** - **23**, and **25** - **26** were not matched against standards. Chemical reagents including glutathione (GSH), NADPH, amodiaquine, diclofenac, dextromethorphan, midazolam, buccetine, clotrimazol, quinidine, desethylamodiaquine, 4'-hydroxydiclofenac, dextrorphan, 6 $\beta$ -hydroxytestosterone, and 1'-hydroxymidazolam were purchased from Sigma-Aldrich (St. Louis, MO) unless noted otherwise. Tacrine, bupropion, *S*-mephenytoin, hydroxybupropion, fluvoxamine, and [<sup>2</sup>H<sub>5</sub>]-*N*-desethylamodiaquine were purchased from Toronto Research Chemicals (Toronto, ON). 4'-Hydroxymephenytoin, [<sup>2</sup>H<sub>6</sub>]-hydroxybupropion, [<sup>2</sup>H<sub>3</sub>]-4'-hydroxymephenytoin, and [<sup>2</sup>H<sub>3</sub>]-dextrorphan were purchased from BD Biosciences (Woburn, MA). [<sup>2</sup>H<sub>3</sub>]-6 $\beta$ -Hydroxytestosterone was procured from Cerilliant (Round Rock, TX), and 1'-hydroxytacrine was obtained from TLC PHARMECHEM (Mississauga, ON). All of the solvents [high-performance liquid chromatography (HPLC) grade] were purchased from Mallinckrodt Baker (Phillipsburg, NJ). Pooled liver microsomes (male cynomolgus monkey, lot 23791, n = 150; male beagle dog, lot 00269, n = 7; male Sprague Dawley rat, lot 85157, n = 164; male human, lot 382898, n = 150) were obtained from BD Gentest (Woburn, MA). Pooled liver S9 (male balb B/C mouse, lot 0810018, n = 200; male beagle dog, lot 90958, n = 6) was purchased from BD Gentest. Pooled liver S9 (cynomolgus monkey, lot 0910273, n = 12; human, lot 0910396, n = 50) was obtained from XenoTech (Lenexa, KS). Pooled liver S9 (Aroclor-1254-induced male Sprague Dawley rat, lot 2572, n = 35) was purchased from Molecular Toxicology, Inc (Boone, NC). Pooled cryopreserved hepatocytes (human, lots GMK,

DMD # 68866

KKO, TNM; rat, lot QSV, n = 20; ICR/CD-1 mouse, lots ONJ, SFZ, AFZ, n = 3; beagle dog, lot OES, n = 5; male cynomolgus monkey, lots OVW, VCE, OAY, n = 3) were obtained from *In Vitro* Technologies (Baltimore, MD). Compound [<sup>14</sup>C]-**1** was prepared as described (Easter *et al.*, submitted). Compound [<sup>3</sup>H]-**1** was prepared by dissolving **1** into acetic acid and treating with 4 equivalents of bromine (1M) in acetic acid. The reaction was stirred overnight and concentrated under vacuum. The resulting dibromo analog was converted to [<sup>3</sup>H]-**1** via debromination with carrier-free tritium gas. The final product [<sup>3</sup>H]-**1** was isolated by HPLC to a purity of 99.3% and a specific radioactivity of 24.5 Ci/mmol.

**Organic Synthesis of Key Metabolites** Procedures outlining the synthesis of metabolites are provided as supplemental material.

**Incubations in Liver Microsomes and Liver S9** Compound [<sup>14</sup>C]-**1** (10 μM) was incubated together with glutathione (GSH; 5 mM) and either liver microsomes (1 mg protein/mL) or liver S9 (2 mg protein/mL) in potassium phosphate buffer (0.1 M, pH 7.4, 1 mL total volume) for 1 h at 37 °C with constant shaking. Alternatively, **1** (10 μM) was incubated together with potassium cyanide (1 mM) and liver microsomes (1 mg protein/mL) in potassium phosphate buffer for 30 min at 37 °C with constant shaking. The samples were preincubated for 3 min, and then reactions were started by addition of NADPH (1 mM). Control incubations without NADPH were done in parallel.

**Incubations in Hepatocytes** Cryopreserved hepatocytes were thawed as recommended by the vendor and diluted to 1.4 to 3.1 million viable cells/mL in a Krebs-Henseleit buffer (pH 7.4) containing sodium hydrogen carbonate (2.2 g/L), HEPES (22.6

DMD # 68866

mM), and calcium chloride (1 mM). Compound [<sup>14</sup>C]-**1** (10 μM) was added to the suspensions and incubated for 4 h at 37 °C under an atmosphere of 5% carbon dioxide.

**Sample Processing** Protein was precipitated by adding an equal volume of ice-cold acetonitrile, followed by vortexing and centrifugation. Supernatants were dried to approximately one-half to one-third of the original volume under nitrogen, and aliquots (90 μL) were analyzed by LC-MS/MS with fraction collection and offline scintillation counting.

**Measurement of Covalent Binding to Protein** Compound [<sup>3</sup>H]-**1** (10 μM) was incubated in triplicate in 96-well plates with pooled rat, dog, monkey or human liver microsomes (1 mg protein/mL) in potassium phosphate buffer (0.1 M, pH 7.4). Incubations were performed both in the presence and absence of GSH (5 mM) and were supplemented with MgCl<sub>2</sub> (3 mM), NADPH (1 mM). Incubations of [<sup>3</sup>H]-imipramine (10 μM, Sigma-Aldrich, St. Louis, MO) were also carried out under identical conditions as a positive control. These mixtures were incubated for 1 h at 37 °C, quenched with 4 volumes of acetone, and then filtered using a Brandel Harvester (Brandel Inc., Gaithersburg, MD). Proteins that precipitated on the filter paper were washed 4 times with 80% methanol. After washing, the filters were placed into scintillation vials, treated with SDS solution (7.5%) and incubated overnight in a water bath at 55 °C. The concentration of protein in each vial was determined using the BCA protein assay, and the rate of tritium decay in each vial was measured over 5 min using a liquid scintillation counter.

**Inhibition of P450 Enzymes** A study was carried out to measure the time-dependent inhibition of P450 enzymes in human liver microsomes by **1**. Assay conditions

DMD # 68866

are summarized in Table 1. Assays were performed in 384-well microplates in a total volume of 30  $\mu$ L. Automated liquid handling equipment (Tecan Genesis 150, Tecan Group Ltd, Hombrechtikon, Switzerland; Velocity 11 BenchCel, Velocity 11, Palo Alto, CA; LabCyte ECHO 550, LabCyte, Sunnyvale, CA; Multidrop Combi, Thermo Fisher Inc., San Jose, CA) was used in all steps of sample preparation. Compound **1** was tested in two independent experiments at final concentrations of 40, 13.3, 4.4, 1.48, 0.49, 0.165, 0.055, 0.018, 0.006, and 0.002  $\mu$ M; positive controls (e.g. 60  $\mu$ M clotrimazole, 40  $\mu$ M quinidine, or 10  $\mu$ M fluvoxamine) were also included in each experiment. Test compounds in DMSO (60 nL) were mixed with the probe substrate in assay buffer (15  $\mu$ L; 100 mM potassium phosphate, pH 7.4, 2 mM MgCl<sub>2</sub>, 1 mM NADPH), then treated with human liver microsomes (15  $\mu$ L) in assay buffer and incubated at 37°C. Reactions were terminated by adding quench buffer (30  $\mu$ L; 94% water, 5% acetonitrile, 1% formic acid) containing reaction-specific internal standards. To assess time-dependent inhibition, test articles in DMSO (60 nL) were pre-incubated with human liver microsomes (15  $\mu$ L) in assay buffer for 30 min at 37°C. Mixtures were then treated with probe substrate in assay buffer (15  $\mu$ L), and the reaction continued. At the end of the incubation, reactions were terminated by adding quench buffer (30  $\mu$ L).

The concentration of specific probe metabolite produced in each well was determined by RapidFire™-Mass Spectrometry (solid phase extraction-MS/MS) and LC-MS/MS (for the CYP3A4-testosterone 6 $\beta$ -hydroxylation reactions). Sample was loaded on-line onto a C4 micro-scale solid phase extraction column (BIOCIUS Life Sciences, Woburn, MA) using water containing 0.01% trifluoroacetic acid and 0.09% formic acid (for CYP1A2, 2C8, 2C9 and 2D6 assays) or water (for CYP2B6 and 2C19 assays) and

DMD # 68866

eluted with acetonitrile containing 0.01% trifluoroacetic acid and 0.09% formic acid (for CYP1A2, 2C8, 2C9 and 2D6 assays) or methanol/water (4:1 v/v) (for the CYP2B6 and 2C19 assays). The eluent was directed to a RapidFire™ 200 HT System and an AB Sciex 4000 QTRAP™ mass spectrometer. For the CYP3A4 assay, 6β-hydroxytestosterone was analyzed using an Agilent Zorbax SB-C18 (150 × 2.1 mm, 5 μm) column (Santa Clara, CA) and a mobile phase consisting of Solvent A (0.1% formic acid in water) and Solvent B (0.1% formic acid in acetonitrile) with a linear gradient delivered at 0.5 mL/min as follows: 20% B for 0.1 min, 20 to 51% B over 3.5 min, 51 to 90% B over 0.1 min, and 90% B isocratic for 0.5 min. The column was then reequilibrated to initial conditions over 0.8 min. Selected reaction monitoring was used for analysis of metabolites and internal standards. The MS/MS data was processed with RapidFire™ peak integration software, and the results were exported into an Excel file for IC<sub>50</sub> calculation.

For analysis of CYP3A4 activity using testosterone as the probe substrate, an aliquot of the reaction mixture (120 μL) was transferred onto a 96-well MultiScreen deep-well filtration plate equipped with 0.45 μm hydrophobic polytetrafluoroethylene membrane (Millipore Co., Billerica, USA). The filtration plate was stacked atop 2 mL 96-well receiver plates, vortexed for 30 sec, and all mixtures were passed through the membrane by centrifugation for 5 min at 2000g. Filtrates were analyzed by LC-MS/MS. The signal intensity of the MS/MS peak corresponding to each metabolite was normalized to the signal of internal standard. Each sample signal ratio was then normalized to signal ratios of the reactions performed in the absence of the test substance (solvent control, 0% inhibition) and in the presence of Inhibitor Cocktail, (background, 100% inhibition). Results were expressed as: percent inhibition = 100(1 - (S-B)/(T-B)),

DMD # 68866

where T = average solvent controls, B = average background, S = sample. The results were then imported into CurveMaster curve fitting software using MathIQ (ID Business Solutions, Ltd., UK) to determine the IC<sub>50</sub>s for each compound.

**Studies Using Animals** All methods were in compliance with the Guide for the Care and Use of Laboratory Animals (Institute of Laboratory Animal Resources, 1996) as adopted by the U.S. National Institutes of Health and approved by the Bristol-Myers Squibb Animal Care and Use Committee. In-life portions of studies using bile-duct-cannulated (BDC) rats and intact animals (mouse, rat, monkey) were completed at Charles River Laboratories (Shrewsbury, MA).

**Intact Mice** Following a fast of approximately 5 to 6.5 h, [<sup>14</sup>C]-**1** was administered orally by gavage (50 mg/kg, 166.7 μCi/kg) in a vehicle of H<sub>3</sub>PO<sub>4</sub> buffer (0.1 M, pH 3)/PEG 400/Povidone K-30/Vitamin E TPGS (75/15/5/5) to 30 male rasH2 mice in Groups 1 and 9 male rasH2 mice in Group 2. The rasH2 strain was selected so that metabolism could be evaluated in the same strain that was used in the carcinogenicity study of **1**. Food was returned to the animals approximately 4 h after dosing. Terminal blood samples were collected into tubes containing K<sub>2</sub>EDTA from mice in Group 1 (5 mice per time point) at 1, 4, 8, 12, 24, and 48 h post-dose. Urine and feces were collected from mice in Group 2 (3 mice per cage) prior to dosing. After dosing, urine was collected over the intervals 0–12, 12–24 h, and then in 24-h intervals through 168 h after dosing. Feces was collected in 24-h intervals through 168 h.

**Intact Rats** Following a fasting period of 11.5 to 12.5 h, [<sup>14</sup>C]-**1** was administered orally by gavage (30 mg/kg, 100 μCi/kg) in a vehicle of H<sub>3</sub>PO<sub>4</sub> buffer (0.1 M, pH 3)/PEG 400/Povidone K-30/Vitamin E TPGS (75/15/5/5) to 27 male SD rats in

DMD # 68866

Group 1, and 3 male SD rats per group in Groups 2 and 3. Food was returned to the animals approximately 4 h after dosing. Terminal blood samples for metabolite profiling were collected into tubes containing K<sub>2</sub>EDTA from animals in Group 1 (3 rats per time point) prior to dosing and at 1, 2, 4, 8, 12, 24, 48, and 96 h post-dose. Blood samples for total radioactivity analysis (TRA) were collected from each animal in Group 3 pre-dose and at 15 time points through 168 h. Urine and feces were collected from the animals in Group 2 pre-dose and over regular intervals through 168 h.

**Intact Monkeys** Following a fasting period of approximately 12.5 h, [<sup>14</sup>C]-**1** was administered orally (30 mg/kg, 40 μCi/kg) in a vehicle of H<sub>3</sub>PO<sub>4</sub> buffer (0.1 M, pH 3)/PEG 400/Povidone K-30/Vitamin E TPGS (75/15/5/5) to 3 male cynomolgus monkeys. Food was returned to the animals approximately 4 h after dosing. Blood samples for TRA were collected into tubes containing K<sub>2</sub>EDTA from each animal pre-dose and at 15 time points through 168 h after dosing. Additional blood samples were collected for metabolite profiling pre-dose and at 1, 4, 8, 12, 24, and 48 h. Urine and feces were collected pre-dose and over regular intervals through 168 h.

**BDC Rats** Following a fasting period of approximately 9 h, [<sup>14</sup>C]-**1** was administered orally (30 mg/kg, 100 μCi/kg) in a vehicle of H<sub>3</sub>PO<sub>4</sub> buffer (0.1 M, pH 3)/PEG 400/Povidone K-30/Vitamin E TPGS (75/15/5/5) to 3 BDC male Sprague Dawley rats. Food was returned to the animals approximately 4 h after dosing. Blood samples were collected into tubes containing K<sub>2</sub>EDTA from each animal pre-dose and at 1, 4, 12, 24, and 48 h post-dose. Bile, urine, and feces were collected pre-dose and over regular intervals through 48 h.

DMD # 68866

**Catheterization of Dog and Monkey Bile Ducts** The procedure for catheterization of dog and monkey bile ducts is provided as supplemental material.

**BDC Dogs** Following a fasting period of approximately 8 h, [<sup>14</sup>C]-**1** was administered orally (50 mg/kg, 20 μCi/kg) in a vehicle of H<sub>3</sub>PO<sub>4</sub> buffer (0.1 M, pH 3)/PEG 400/Povidone K-30/Vitamin E TPGS (75/15/5/5) to 3 BDC male beagle dogs. Food was returned to the animals approximately 4 h after dosing. Blood samples were collected into tubes containing K<sub>2</sub>EDTA pre-dose and at 0.5, 1.5, 4, 8, 24, 48, and 72 h post-dose. Bile and urine samples were collected over the intervals of 0-8, 8-24, 24-48, and 48-72 h post-dose. Similarly, feces samples were collected over the intervals of 0-24, 24-48, and 48-72 h post-dose.

**Placement of Vascular Access Ports in Monkeys** The procedure for the placement of vascular access ports in monkeys is provided as supplemental material.

**BDC Monkeys** Following a fasting period of approximately 8 h, [<sup>14</sup>C]-**1** was administered orally (100 mg/kg, 40 μCi/kg) in a vehicle of H<sub>3</sub>PO<sub>4</sub> buffer (0.1 M, pH 3)/PEG 400/Povidone K-30/Vitamin E TPGS (75/15/5/5) to 3 BDC male cynomolgus monkeys. Food was returned to the animals approximately 4 h after dosing. Blood samples were collected into tubes containing K<sub>2</sub>EDTA pre-dose and at 0.5, 2, 4, 8, 24, 48, and 72 h post-dose. Bile and urine samples were collected over the intervals of 0-8, 8-24, 24-48, and 48-72 h post-dose. Feces were collected over the intervals of 0-24, 24-48, and 48-72 h post-dose.

**Processing of Animal Samples** Upon collection, blood samples were placed on ice and centrifuged for 15 min at 1000 g to separate plasma. Equal volumes of plasma from each animal in a particular study were combined to create a pooled plasma sample

DMD # 68866

for each time point. Pooled plasma samples were treated with 2 volumes of methanol/acetonitrile (50:50 v/v) and centrifuged at 3500 g for 30 min. Supernatants were collected, and the pellet was extracted twice with 2 volumes of methanol:acetonitrile:water (25:25:50 v/v/v). The supernatants from each extraction were combined and evaporated to small volume under nitrogen. Any insoluble material was removed by centrifugation at 19,000 g for 15 min, and the concentrated extracts (20-90  $\mu$ L) were analyzed by LC-MS/MS. Feces samples were homogenized (4 mL/g) with acetonitrile/water (1/1) during studies using BDC rats and intact animals (mouse, rat, monkey). Feces were diluted by 3 mL/g in the BDC monkey and BDC dog studies. Pooled feces homogenates in each study were prepared by mixing a constant percentage (2-30%) of feces by weight (intact mouse, intact rat, BDC rat, and intact monkey) or by volume (for BDC monkey and BDC dog) from each time interval, exclusive of the pre-dose samples. Pooled fecal homogenates were extracted with 2 volumes of acetonitrile/methanol (1/1), vortexed (3500 rpm) for 30 min, sonicated for 5 min, and centrifuged at 19,000 g for 15 min. After the supernatant was removed, the extraction was repeated twice with 2 volumes of methanol/acetonitrile/water (1/1/2). The supernatants from each extraction step were combined and evaporated to small volume under nitrogen, and aliquots (20-90  $\mu$ L) were analyzed by LC-MS/MS. In studies using BDC animals, pooled bile samples were prepared in similar fashion to the pooled fecal homogenates. Pooled bile samples were centrifuged at 13,000 rpm for 5 min, and aliquots (25-90  $\mu$ L) of the supernatant was analyzed by LC-MS/MS.

**TRA Measurement** Aliquots of the bile, plasma, or urine were mixed with liquid scintillation cocktail (Ecolite or Permafluor E+), and the amount of radioactivity was

DMD # 68866

measured using either a Packard Tri-Carb 2250 liquid scintillation counter (PerkinElmer Life and Analytical Sciences) or a Model LS 6000 liquid scintillation counter (Beckman Instruments, Inc., Fullerton, California). Fecal homogenates from intact animals (mouse, rat, monkey) and BDC rats were dried at ambient temperature for at least 4 h and burned in a Model 307 sample oxidizer (PerkinElmer, Inc., Boston, Massachusetts). The resulting  $^{14}\text{CO}_2$  was trapped in Carbo-Sorb E (PerkinElmer, Inc.), mixed with scintillation fluid, and analyzed by liquid scintillation counting. Portions of feces homogenates (0.05 – 0.15 g) from BDC monkeys and BDC dogs were mixed with Soluene 350 in a 25-mL glass scintillation vial and incubated overnight at 60 °C with gentle shaking. After cooling, 30% hydrogen peroxide (0.2 mL) and Ecolite (15 mL) were added, and the resulting sample was analyzed by liquid scintillation counting.

**LC-MS/MS and Radiochromatographic Analysis** Chromatographic separations were carried out using an Agilent or Shimadzu HPLC system (binary pump, autosampler and a photodiode array UV detector) and a Phenomenex (Torrance, CA) Luna C18 column (4.6 × 150 mm, 5 μm) that was maintained at ambient temperature. The column temperature was ambient. The mobile phase of 10-mM ammonium acetate (pH 5) in water (solvent A) and acetonitrile (solvent B) was delivered at a flow rate of 1.0 mL/min with gradient conditions as follows: 5% to 32% B over 18 min, 32% B for 27 min, 32% to 55% B over 15 min, 55% to 80% B over 5 min, and 80% B for 3 min. The column was then reequilibrated to initial conditions over 6 min. The HPLC eluent was directed through a splitter so that approximately 20% of the eluate was analyzed by positive-ion electrospray MS and MS/MS using a Thermo (San Jose, CA) LTQ or LTQ Orbitrap mass spectrometer. Metabolites were identified based on HPLC retention time, elution order,

DMD # 68866

and LC/MS<sup>n</sup> fragmentation patterns compared to those of **1** and other available reference standards. Compound **3** was also isolated for NMR analysis. For quantification of radioactivity in samples, the remaining 80% of the HPLC eluate was collected in regular intervals (12 s) into Deepwell LumaPlate<sup>TM</sup> 96-well plates (PerkinElmer Life and Analytical Sciences, Boston, MA) using a Gilson Model FC 204 fraction collector (Gilson Medical Electronics, Middletown, WI). Fractions were dried in an Automatic Environmental Speed Vac (Savant, Holbrook, NY) and counted for radioactivity for 10 min using a Packard TopCount NXT<sup>TM</sup> Scintillation and Luminescence Counter (PE Life Sciences, Downers Grove, IL). A background of 2 to 3 counts per min was subtracted from the value of each fraction, and metabolite profiles (radiochromatograms) were drawn by plotting the resulting net counts-per-minute values vs. time using Microsoft<sup>®</sup> Excel. The relative abundance of each metabolite was calculated by summing the radioactivity in the fractions corresponding to the metabolite and dividing by the net (background-subtracted) radioactivity collected during the HPLC run. In certain cases minor metabolites corresponding to small peaks in the radiochromatogram could not be identified. In these cases, the reported sum of radioactive metabolites is less than 100% of the total radioactivity in the sample.

**Isolation of 3 from Rat Bile** A composite sample of BDC rat bile (55 mL) from two animals was extracted twice with equal volumes of ethyl acetate. The ethyl acetate phase was collected and evaporated to dryness under nitrogen at room temperature. The ethyl acetate extract was re-dissolved in 0.5 mL methanol, centrifuged to remove insoluble matter, and the supernatant was concentrated under nitrogen. This methanol treatment procedure was repeated two additional times. The resulting clear supernatant

DMD # 68866

(100  $\mu$ L concentrate) was processed by semi-preparative HPLC in multiple injections (30  $\mu$ L aliquots) using an Agilent HP-1100 HPLC workstation and a Waters Sunfire C-18 (5  $\mu$ m) 4.6  $\times$  150 mm column. The mobile phase consisted of 10-mM ammonium acetate (pH 5) and 5% acetonitrile (solvent A) and acetonitrile (solvent B) with a linear gradient as follows: 15 to 85% B over 25 min, 85% B isocratic for 5 min, then a return to initial conditions over 2 min. The flow rate was 1.2 mL/min. Eluent from the column was routed in-line to an Agilent photodiode array detector (254 nm) and then to an Agilent MSD operated in positive ion electrospray mode. Fractions were collected in parallel using a Gilson 215 fraction collector (time-based protocol, left 80 format) into a 96-deep-well Beckman polypropylene block (0.4 min/fraction for 32 min). The metabolite of interest, **3** ( $m/z$  755), eluted at 10.4 minutes under these chromatographic conditions. Fractions containing **3** were pooled and evaporated overnight under nitrogen at room temperature. The isolated metabolite was then re-dissolved in 50  $\mu$ L of DMSO- $d_6$  and transferred to a 1.7-mm capillary tube.

**NMR Spectroscopy.** The isolated metabolite **3** was analyzed using a Varian Inova 600 MHz NMR spectrometer equipped with a 5-mm triple-resonance cold probe. The temperature of the probe was maintained at 25  $^{\circ}$ C during all experiments unless noted otherwise. A proton spectrum was acquired, with a spectral width of 9607.3 Hz, consisting of 23,643 data points and 64 scans. Before the Fourier transformation, the dataset was zero-filled to 65,536 (64K) points and a line broadening of 0.5 Hz was applied. The 2-dimensional  $^1\text{H}$ - $^{13}\text{C}$  correlation [heteronuclear single quantum correlation (HSQC)] experiment was performed with 9,611  $\times$  25,632 ( $^1\text{H} \times ^{13}\text{C}$ ) Hz and 2,048  $\times$  96 points. For each of the 96 free-induction decay cycles (FIDs), 256 scans were used.

DMD # 68866

Before Fourier transformation, squared cosine window functions for each dimension and a linear prediction for the indirect  $^{13}\text{C}$  dimension were applied. The final spectral size was  $2048 \times 2048$  points.  $^1\text{H}$ - $^1\text{H}$  correlation spectroscopy (COSY), total correlation spectroscopy (TOCSY) and transverse rotating frame Overhauser enhancement spectroscopy (TROESY) experiments were acquired with 9,612 Hz in both dimensions and  $2048 \times 96$  points. During the acquisition of these data, residual water was suppressed with low-power radiation during the relaxation delay. For each FID in these datasets, 128 scans were used. The final sizes of these spectra were  $2048 \times 2048$ . Linear predictions and cosine window functions were applied before the Fourier transformation. To assist in the interpretation of NMR spectra, ACD/HNMR Predictor and ACD/CNMR Predictor (Advanced Chemistry Development, Toronto, ON) were used.

DMD # 68866

## Results

Compound [ $^{14}\text{C}$ ]-**1** was incubated with liver microsomes (dog, human, monkey, rat), liver S9 (dog, human, monkey, mouse, Aroclor-induced rat), and hepatocytes (dog, human, monkey, mouse, rat). It was also administered p.o. to intact animals (mice, monkeys, rats) and BDC animals (dogs, monkeys, rats). Data that was recorded during positive-ion electrospray LC-MS/MS analysis of **1** and its metabolites is summarized in Table 2. Proposed biotransformation pathways of **1** are illustrated in Fig. 2.

The *in vitro* metabolite profiles of [ $^{14}\text{C}$ ]-**1** were similar across species, with few differences observed among the hepatic matrices that were used to generate metabolites (Table 3). Radiochromatograms that were acquired following the incubation of [ $^{14}\text{C}$ ]-**1** (10  $\mu\text{M}$ ) with liver microsomes, liver S9, and suspended hepatocytes are available as supplemental materials. In summary, most metabolites observed during *in vitro* studies were formed via oxidative processes, and the main metabolic pathways that occurred in hepatocytes were also observed in liver S9 and microsomes. Compounds **2**, **3**, and **4** were among the most abundant metabolites and were present in all species and matrices. Most metabolites were formed in NADPH-dependent fashion, although **4** was also detected in incubations without NADPH at levels that were approximately 70% lower across species (data not shown). This observation demonstrated a degree of involvement by P450 in catalyzing the formation of **4**. Whereas **2** was relatively abundant in human liver incubations *in vitro*, it did not turn out to be a major metabolite in humans (Farley, 2015). No GSH conjugates were found in any matrix, and no cyano adducts were found in incubations with liver microsomes supplemented with potassium cyanide. Additionally,

DMD # 68866

prominent metabolites such as **3** were observed in the presence of trapping agents (e.g. GSH, cyanide) in the incubations with liver microsomes.

**Covalent Binding to Protein** Also, a study was performed to measure the amount of radioactivity covalently bound to protein after incubations of [<sup>3</sup>H]-**1** and [<sup>3</sup>H]-imipramine (positive control) with liver microsomes (human, monkey, rat) and NADPH. The results of this study, summarized in Table 4, indicated that levels of irreversible binding to protein across species were low and below those of the positive control. Although rates were attenuated in the presence of GSH in certain species (mouse, monkey), no GSH conjugates were detected. The absence of such conjugates is interpreted to mean that the differences in rates, with and without GSH, were small enough to preclude detection of a GSH conjugate that might have accounted for these differences. Hence, while the results provide evidence that GSH conjugates might have formed at very low levels, none were detected directly by LC-MS. Rates of binding by [<sup>3</sup>H]-imipramine measured in the study were comparable to reported values (Evans *et al.*, 2004).

**Inhibition of P450 Enzymes** Compound **1** was evaluated as a time-dependent inhibitor of P450 enzymes in human liver microsomes. The results of these experiments demonstrated that **1** did not inhibit CYP1A2, CYP2B6, CYP2C8, CYP2C9, CYP2C19, or CYP2D6, either with or without a 30-min preincubation (all IC<sub>50</sub>s > 40 μM). In contrast, **1** was found to be a weak to moderate inhibitor of CYP3A4, as evidenced by time-dependent inhibition of midazolam 1'-hydroxylation (IC<sub>50</sub> = 31.8 μM without preincubation and IC<sub>50</sub> = 13.5 μM with preincubation) and inhibition of testosterone 6β-

DMD # 68866

hydroxylation ( $IC_{50} = 11.0 \mu\text{M}$  without preincubation and  $IC_{50} = 8.9 \mu\text{M}$  with preincubation).

**Recovery of Radioactivity from Animals** The mass-balance of radioactivity after oral administration of [ $^{14}\text{C}$ ]-**1** to intact animals (mice, monkeys, rats) and BDC animals (dogs, monkeys, rats) is provided as supplementary material. In intact animals, most of the administered radioactivity was recovered (90-96% of dose), with the majority of radioactivity excreted in the feces (69-91%) and only a small portion in the urine (< 2%) or remaining in the carcass (< 2%). The relatively low recovery of radioactivity in feces from intact monkeys (72%) was attributed to soft feces that could not be completely collected, since approximately 20% of the dose was recovered in cage debris and was of probable fecal origin. Total recovery of radioactivity was lower in BDC animals (63-84% of dose) because of the shorter collection time. Bile and feces both represented major routes for the excretion of radioactivity in BDC animals, and together they accounted for the majority (55-81%) of radioactivity administered.

**Metabolites in Plasma** The distribution of radioactivity among [ $^{14}\text{C}$ ]-**1** and its metabolites in plasma, following oral administration to animals, is summarized in Table 5. Radiochromatograms are also provided as supplemental materials. Plasma metabolite profiles were qualitatively similar across species. Unchanged [ $^{14}\text{C}$ ]-**1** comprised the majority (74-94%) of circulating radioactivity. Compound **3** was a major metabolite in monkey plasma and was also detected in plasma from all other animals. All other metabolites were minor, with each representing < 10% of circulating radioactivity.

**Metabolites in Excreta** Metabolite profiles of pooled feces and bile following oral administration of [ $^{14}\text{C}$ ]-**1** as a single dose to animals are summarized in Table 6, and

DMD # 68866

corresponding radiochromatograms are provided as supplemental materials. Metabolite profiles in feces were qualitatively similar across the species. Compound [<sup>14</sup>C]-**1** was the main drug-related component recovered in feces (all species) and was also the main compound in bile (rats, dogs). In contrast, **3** was the most abundant drug-related compound in bile from monkeys. Compound **4**, which was formed *in vitro* across species, was a common component of excreta with levels ranging from 0.9 to 5.9% in feces and 0.2 to 2.2% in bile. Compound **8**, a minor metabolite *in vitro*, was relatively abundant in rodent feces with levels reaching 7.3% (mouse) and 9.4% (rat) over an extended collection period.

**Elucidation of the Structures of Metabolites.** Positive-ion electrospray MS/MS product ions of **1** were generated via CID and analyzed using a Thermo LCQ Deca XP ion trap mass spectrometer. Since **1** possesses a  $C_2$  axis of symmetry, most fragmentation pathways could be attributed to either of two equivalent sites. The monoisotopic mass-to-charge ratios and proposed sites of fragmentation leading to these product ions are illustrated in Fig. 3A. Since the  $C_2$  symmetry of **1** was disrupted during biotransformation, the MS/MS product-ion spectra of metabolites were characterized by pairs of ions (with the intervening space equal to the overall mass shift) in instances where an operative fragmentation plane lay between the symmetry axis and the site of modification. These observations were used to assist in elucidating the structures of metabolites of **1**.

As examples of how tandem mass spectrometry was used to assign the structures of metabolites, product-ion MS/MS spectra of the metabolites **2**, **3**, and **4** are shown in Fig. 3B-D. The MS/MS spectrum of **2** included a pair of ions of  $m/z$  592 (which was also

DMD # 68866

observed in the MS/MS spectrum of **1**) and 598 (not observed in the MS/MS spectrum of **1**) that differed by the mass of a single oxygen atom introduced during metabolism.

These ions were formed by neutral losses of the two methyl carbamate valine moieties, one of which bore the oxygen atom and the other of which did not. The pair of ions thus served as a signal that the site of metabolism lay outward from the fragmentation plane with respect to the  $C_2$  symmetry axis. Since the most likely soft spots for oxidation leading to the formation of **2** were inferred to be on the valine moiety, standards of **2** and its diastereomer **39** were synthesized chemically (synthetic procedures are provided as supplemental materials). The MS/MS spectra of both **2** and **39** resembled the spectrum of the metabolite detected *in vitro*. However, these standards were separable by HPLC, and only the retention time of the standard of **2** matched that of the metabolite.

In the MS/MS product ion spectra of **3**, the two most intense peaks of  $m/z$  580 and 581 were interpreted to result from neutral losses of water (18 u) and ammonia (17 u), respectively, from the “devalinated” product ion of  $m/z$  598 that was formed via amide-bond cleavage (N7–C17). These data suggested monooxidation of the pyrrolidine ring. Although the product ion spectrum of **3** was similar to those of **6** or **7**, the LC retention time of **3** differed from those of these standards in either of their diastereomeric forms (not shown), precluding the possibility that either C9 or C10 (or C41 or C42) were sites of oxidation leading to the formation of **3** and instead implying the site of oxidation was C6 or C8. The structure of **3** was thus further elucidated by NMR on a sample isolated from rat bile (see next section).

Compound **4** formed a protonated molecule of  $m/z$  681 during positive-ion electrospray MS, suggesting removal of the methyl carbamate. Product ions that were

DMD # 68866

observed during MS/MS were also consistent with this assignment. The MS/MS spectrum exhibited a pair of ions of  $m/z$  524 and 582, equal to the separation between the masses of **1** and **4** and signaling heteroatom dealkylation associated with the valine moiety. As noted above, the formation of **4** was at least partially dependent on NADPH. Such reactions have been reported previously as potentially mediated by P450 enzymes (Berndt *et al.*, 1995; Ghosal *et al.*, 2011).

Structures of the remaining metabolites of **1** were proposed, again following the logic described above around the spectral interpretation of metabolites of symmetrical compounds. The data supporting these assignments are summarized in Table 2. In addition to the interpretation of MS/MS results shown here, LC-MS/MS analysis of synthetic standards of **2**, **3**, **4**, **6**, **7** and **8** helped to verify the identity of these metabolites in biological samples. Structures of the remaining metabolites were proposed based on LC-MS/MS data alone.

**Characterization of 3 by NMR.** Although the isolated metabolite **3** eluted as a single component using the HPLC method described, there were two discrete  $^1\text{H}$  and  $^{13}\text{C}$  resonances for *C5*, *C8*, *H8*, *H25*, and *NH7*. Each represented one-half of the theoretical integration, suggesting the presence of a pair of conformers or diastereomers. Compared to the  $^1\text{H}$  NMR spectrum of **1**, the spectrum of **3** exhibited an additional pair of resonances at 5.52 ppm and 5.48 ppm (*H8*) (Fig. 4). These two resonances correlated with carbinol carbons (*C8*) of 76.6 ppm and 77.6 ppm, respectively, as illustrated in the HSQC spectra in Fig. 5. A number of diagnostic through-bond and through-space correlations are summarized in Fig. 6. Among them, the carbinol methine (*H8*) demonstrated a 2-bond  $^1\text{H}$ - $^1\text{H}$  correlation with the methylene *H9* (2.1 ppm) in the COSY

DMD # 68866

spectrum and a 5-bond  $^1\text{H}$ - $^1\text{H}$  correlation to the methine *H6* (4.9 ppm) in the TOCSY spectrum. *H6* also correlated to an exchangeable proton *H7* (8.3 ppm) in the COSY spectrum. These observations suggested that **3** retained the intact *H6/C6*–*C2* linkage from **1** and that *H8*, *H9*, *H6* and *H7* belonged to the same substructure (Fig. 6A).

Additional NMR data were collected subsequently on a synthetic standard of **3**. The  $^1\text{H}$  (Fig. 4) and  $^1\text{H}$ - $^{13}\text{C}$  HSQC (Fig. 5) spectra of the standard were found to match those of the isolated metabolite, indicating that the synthetic product was the same compound isolated from the rat bile. The greater quantity of the synthetic material enabled additional observations of **3** using NMR. For example, the TROESY data showed extensive through-space correlations (NOEs) for a network of protons and enabled the characterization of a tetrahydroimidazolo[1,2-*a*]pyridine partial structure (Fig. 6B). Finally, the gHMBC spectra revealed multiple key long-range through-bond correlations from *H5*, *H6*, and *H8* to *C2* (Fig. 6C), confirming the proposed structure for **3** (Fig. 2).

Finally, a doubling of  $^1\text{H}$  and  $^{13}\text{C}$  resonances of *H6/C6*, *H25* and *NH7* was apparent. In order to investigate this observation further, additional experiments were performed including the acquisition of a ROESY spectrum and  $^1\text{H}$  spectra at various temperatures (10, 20, 30 and 40°C). In the ROESY spectrum (not shown), no exchange cross-peaks were observed between these  $^1\text{H}$  pairs. In the  $^1\text{H}$  spectra, no narrowing or broadening of the  $^1\text{H}$  pairs was observed as a function of temperature.

DMD # 68866

## Discussion

Compound **1** is a first-in-class, selective inhibitor of the NS5A replication complex that is marketed as a treatment for hepatitis C virus infection. This compound represents the product of a medicinal chemistry campaign described previously (Romine *et al.*, 2011; St. Laurent *et al.*, 2012; Lopez *et al.*, 2013; St. Laurent *et al.*, 2013; Belema *et al.*, 2013; Belema *et al.*, 2014a; Belema *et al.*, 2014b). The present studies were completed during the discovery and early development of **1** in support of its candidacy for clinical development.

During the *in vivo* biotransformation experiments, doses in excess of the clinical dose were studied. These doses were selected to mimic toxicologic doses and help determine which metabolites might be represented during nonclinical safety studies. Following oral administration of [<sup>14</sup>C]-**1** as a single dose to intact animals (mouse, monkeys, rats), the majority of radioactivity was excreted in the feces. Studies in BDC animals (dogs, monkeys, rats) also demonstrated important contributions from biliary excretion in the disposition of **1**, whereas urinary excretion of radioactivity was minor. Unchanged **1** was a prominent component in feces (across species) and bile (rat, dog). Qualitatively similar metabolite profiles were observed in the feces and bile across species. The only major metabolite that represented > 10% of total excreted radioactivity (monkey, BDC rat) was **3**. Compound **8**, which represented 7.3% (mouse) and 9.4% (rat) of the drug-related material excreted in feces, was more abundant *in vivo* than might have been predicted based on the *in vitro* data, although it is not known whether metabolic processes inside the gut might have contributed to its formation. In contrast, metabolites such as **2** and **4** that were detected *in vitro* across species turned out to be minor products

DMD # 68866

in excreta following the administration of [ $^{14}\text{C}$ ]-**1** in animals. Since **3** was also the main metabolite of **1** in human liver microsomes, and results between *in vitro* and *in vivo* models were generally in good agreement, the formation of **3** was also anticipated to be the main pathway for the metabolism of **1** in humans.

Since the MS/MS spectrum of **3** (Fig. 2C) did not provide sufficient information to allow the regiochemistry of mono-oxidation to be assigned, **3** was isolated from rat bile for additional structural characterization using NMR. Despite the low sample concentration and spectral complexity, the spectra acquired were interpretable and provided evidence for the site of oxidation. In comparison to the NMR data of **1**, the  $^1\text{H}$  chemical shift (5.48 and 5.52 ppm) of the new methine proton in the isolated metabolite **3** were consistent with those of a CH group bound to both oxygen and nitrogen. Since the mono-oxidation of methylene or aromatic sites other than C8 would not have resulted in  $^1\text{H}$  resonances at 5.5 ppm, it was thought initially that **3** may have formed by simple hydroxylation of C8. The two discrete resonances that were ascribed to H8/C8 were thought to represent two diastereomers that might have been formed by rebound of oxygen from the P450 active site onto either face of the pyrrolidine ring. The possibility that these resonances could alternatively be attributed to tautomers, representing open and closed forms of the pyrrolidine ring that interchanged slowly with respect to the NMR time scale, was another option that was considered. However, the observation of a  $^1\text{H}$ - $^1\text{H}$  correlation between H6 (4.9 ppm) and an exchangeable proton H7 (8.3 ppm) in the COSY spectrum (correlations illustrated in Fig. 6) of **3** provided the first evidence that precluded the possibility of an intact pyrrolidine ring, since an exchangeable proton would not have been assignable in this structure. Since the small amount of **3** that was

DMD # 68866

isolated from the rat bile sample precluded additional experiments to fully investigate the structure of **3** and the cause of the doubling of *H8/C8* resonances, preparation of a synthetic standard of **3** was undertaken.

A synthetic pathway to **3** was devised with the intention of introducing a hydroxyl group onto *C8*, in keeping with the structure that was proposed following NMR analysis of the isolated metabolite. Subsequent analysis of the synthetic material gave <sup>1</sup>H-NMR spectra that were of higher quality, and LC-MS/MS data that were consistent with those obtained previously during analysis of the isolated material, suggesting that the isolated and synthetic compounds were the same. Additional 2D-NMR spectral data from TROESY and gHMBC experiments enabled the continued characterization of the tetrahydroimidazo[1,2-*a*]pyridine moiety (Fig. 6) and complete structure of **3**. The formation of **3** was rationalized as a result of P450-mediated  $\delta$ /*C8*-oxidation of the pyrrolidine moiety and ring-opening to an aminoaldehyde intermediate, followed by an intramolecular reaction between the aldehyde and a proximal imidazole nitrogen *N1*. The structure of **3** also explained the <sup>13</sup>C chemical shift differences between *C6* and *C8*. Specifically, using ACD software for the prediction of <sup>1</sup>H and <sup>13</sup>C chemical shifts based on NMR data of similar sub-structures, the <sup>13</sup>C chemical shift of *C8* (54 ppm) was shown to be consistent with its presence in a 5-membered (*i.e.* pyrrolidine) ring, whereas the <sup>13</sup>C chemical shift of *C6* (44 ppm) was consistent with its inclusion in a 6-membered (piperidine) ring. Similarly, the observed <sup>13</sup>C chemical shift of *C8* (77 ppm) was closer to the predicted chemical shift in the revised structure containing a piperidine ring (77 ppm) than in the preliminary structure containing a pyrrolidine ring (80 ppm). The NMR data of the synthetic standard of **3** also suggested the presence of two isomers of equal

DMD # 68866

population. To investigate this point further, a ROESY spectrum and multiple  $^1\text{H}$  spectra were acquired across temperatures. The results of these experiments suggested that the isomers were related structurally but were not interchangeable on a conformational basis. This observation was consistent with the mechanism proposed for the formation of **3**, where *N1* carries out nucleophilic attack on the nascent aldehyde at *C8* and produces a mixture of diastereomers with the hydroxyl group oriented differently between them. This model was supported further by the observation of a single, weak correlation between *H8* and *C2* in the gHMBC spectrum, since only one of the two diastereomers maintains a dihedral angle along *H8-C8-N1-C2* that gives rise to the *H8-C2* coupling constant and the corresponding long-range correlations. Thus, the evidence supported the structure of **3** shown in Fig. 2 with isomers differing by the configuration of *C8*.

The observation of **3** following incubations of **1** in liver microsomes suggested that the intramolecular reaction of the proposed aminoaldehyde intermediate leading to **3** was favored thermodynamically over bimolecular reactions with biological nucleophiles. This explanation was supported by the rates of irreversible binding to protein that were measured during incubations of [ $^3\text{H}$ ]-**1** in liver microsomes, where reaction with a diverse set of nucleophiles could be accounted for. The measured rates were lower than the positive control and also lower than historic controls run in the same assay (BMS, data on file). Additionally, the levels of binding represented a fraction of the dose administered and were orders of magnitude lower than the percentage converted to **3**. The explanation that rearrangement was favored over bimolecular reaction was also supported by the observation that time-dependent inhibition of CYP3A4 was weak. Indeed, CYP3A4 was involved in the formation of **3** (data not shown). While the formation of a reactive

DMD # 68866

aminoaldehyde intermediate would provide a plausible explanation for the time-dependent inhibition, no attempt to identify covalently modified tryptic fragments of CYP3A4 was made in light of the weakness of the inhibition. Generally, reactions between aldehydes and amino acid side-chains such as lysine and histidine are known (Kalgutkar *et al.*, 2005) and are enthalpically accessible in the absence of competing pathways. Here, however, the relative reaction energies appear to be entropically governed, with the unimolecular reaction (favored) benefiting from limited ground-state freedom and the bimolecular reaction (disfavored) requiring energy expenditure via the adoption of an ordered state and concomitant loss in translational / rotational freedom. This concept is an important aspect of reaction mechanisms (Carey and Sundberg, 1990). The formation of **3** therefore could be understood to mitigate any effects associated with the bimolecular reactivity of the aminoaldehyde intermediate.

In conclusion, disposition of **1** occurred mainly via biliary and intestinal excretion of **1**, and biliary and intestinal excretion of metabolites: predominantly **3** (rat and monkey). The metabolite profile in plasma of nonclinical species included **1** as the main drug-related compound and modest levels of metabolites. Cytochromes P450 were implicated as the most important enzymes in the metabolism of **1** across nonclinical animal species. Pathways for the oxidative biotransformation of **1** included  $\delta$ -oxidation of the pyrrolidine moiety and rearrangement to yield **3**. Although this pathway was postulated to result in the formation of a transient aldehyde, evidence from the covalent binding study and P450 inhibition assays suggested that this intermediate possessed a limited tendency to react with biological nucleophiles. Therefore, this biotransformation

DMD # 68866

profile was considered to be acceptable and supportive of the advancement of **1** into development for the treatment of chronic HCV infection.

DMD # 68866

### **Acknowledgments**

The authors gratefully acknowledge Tatyana A. Zvyaga for assistance with the P450 inhibition experiments.

DMD # 68866

### **Authorship Contributions**

Participated in research design: Li, Liu, Huang, Lopez, Belema, Hamann, Gao, Zhu, Shu, Humphreys, Johnson

Conducted experiments: Li, Liu, Zhao, Lopez, Leet, Fancher, Nguyen, Caceres-Cortes, Chang, Ma, Johnson

Contributed new reagents or analytic tools: Liu, Huang, Lopez, Nguyen, Goodrich, Easter, Hong, Caceres-Cortes, Belema

Performed data analysis: Li, Liu, Zhao, Huang, Leet, Chang, Johnson

Wrote or contributed to the writing of the manuscript: Li, Leet, Fancher, Shu, Humphreys, Johnson

DMD # 68866

## References

- Belema M, Nguyen VN, St Laurent DR, Lopez OD, Qiu Y, Good AC, Nower PT, Valera L, O'Boyle II DR, Sun J-H, Liu M, Fridell RA, Lemm JA, Gao M, Knipe JO, Meanwell NA, Snyder LB (2013) HCV NS5A replication complex inhibitors. Part 5: discovery of potent and pan-genotypic glycinamide cap derivatives. *Bioorg Med Chem Lett* 23:4428-4435.
- Belema M, Nguyen VN, Romine JL, St. Laurent DR, Lopez OD, Goodrich J, Nower P T, O'Boyle DR II, Lemm JA, Fridell RA, Gao M, Fang H, Krause RG, Wang YK, Oliver AJ, Good AC, Knipe JO, Meanwell NA, Snyder LB (2014a) Hepatitis C virus NS5A replication complex inhibitors. Part 6: discovery of a novel and highly potent biarylimidazole chemotype with inhibitory activity toward genotypes 1a and 1b replicons. *J Med Chem* 57:1995-2012.
- Belema M, Nguyen VN, Bachand C, Deon DH, Goodrich JT, James CA, Lavoie R, Lopez OD, Martel A, Romine JL, Ruediger EH, Snyder LB, St Laurent DR, Yang F, Zhu J, Wong HS, Langley DR, Adams SP, Cantor GH, Chimalakonda A, Fura A, Johnson BM, Knipe JO, Parker DD, Santone KS, Fridell RA, Lemm JA, O'Boyle II DR, Colonna RJ, Gao M, Meanwell NA, Hamann LG (2014b) Hepatitis C Virus NS5A Replication Complex Inhibitors: The Discovery of Daclatasvir. *J Med Chem* 57:2013-2032.
- Berndt A, Hoffmann C, Richter K, Oertel R, Vierkant A, Siegmund W (1995) Triacizine disposition in healthy volunteers with reference to the debrisoquine oxidation phenotype. *Br J Clin Pharmacol* 40:287-288.
- Berry MN, Friend DS (1969) High-yield preparation of isolated rat liver parenchymal cells. *J Cell Biol* 43:506-520.
- Blight KJ, Kolykhalov AA, Rice CM (2000) Efficient initiation of HCV RNA replication in cell culture. *Science* 290:1972-1974.

DMD # 68866

Bressanelli S, Tomei L, Roussel A, Incitti I, Vitale RL, Mathieu M, De Francesco R, and Rey FA (1999) Crystal structure of the RNA-dependent RNA polymerase of hepatitis C virus. *Proc Natl Acad Sci USA* 96:13034-13039.

Carey FA and Sundberg RJ (1990) *Advanced Organic Chemistry*, 3rd ed. pp 194-196. Plenum Press, New York.

Chayama K, Takahashi S, Toyota J, Karino Y, Ideda K, Ishikawa H, Watanabe H, McPhee F, Hughes E, Kumada H (2012) Dual therapy with the nonstructural protein 5A inhibitor, daclatasvir, and the nonstructural protein 3 protease inhibitor, asunaprevir, in hepatitis C virus genotype 1b-infected null responders. *Hepatology* 55:742-748.

Easter JA, Burrell RC, Bonacorsi Jr SJ (submitted) Synthesis of isotopically labeled daclatasvir for use in human clinical studies. *J Label Compd Radiopharm*

Evans D, Watt AP, Nicoll-Griffith DA, Baillie TA (2004) Drug-protein adducts: an industry perspective on minimizing the potential for drug bioactivation in drug discovery and development. *Chem Res Toxicol* 17:3-16.

Farley JJ (2015) Daklinza: Full prescribing information. Reference ID: 3797248; [www.accessdata.fda.gov/drugsatfda\\_docs/label/2015/206843Orig1s000lbl.pdf](http://www.accessdata.fda.gov/drugsatfda_docs/label/2015/206843Orig1s000lbl.pdf).

Gao M, Nettles RE, Belema M, Snyder LB, Nguyen VN, Fridell RA, Serrano-Wu MH, Langley DR, Sun JH, O'Boyle II DR, Lemm JA, Wang C, Knipe JO, Chien C, Colonno RJ, Grasela DM, Meanwell NA, Hamann LG (2010) Chemical genetics strategy identifies an HCV NS5A inhibitor with a potent clinical effect. *Nature* 465:96-100.

Ghosal A, Lu X, Penner N, Gao L, Ramanathan R, Chowdhury SK, Kishnani NS, Alton KB (2011) Identification of human liver cytochrome P450 enzymes involved in the

DMD # 68866

metabolism of SCH 530348 (Vorapaxar), a potent oral thrombin protease-activated receptor 1 antagonist. *Drug Metab Dispos* 39:30-38.

The Global Burden of Hepatitis C Working Group (2004) Global burden of disease (GBD) for hepatitis C. *J Clin Pharmacol* 44:20-29.

Institute of Laboratory Animal Resources (1996) *Guide for the Care and Use of Laboratory Animals* 7th ed. Institute of Laboratory Animal Resources, Commission on Life Sciences, National Research Council, Washington DC.

Kalgutkar AS, Gardner I, Obach RS, Shaffer CL, Callegari E, Henne KR, Mutlib AE, Dalvie DK, Lee JS, Nakai Y, O'Donnell JP, Boer J, Harriman SP (2005) A comprehensive listing of bioactivation pathways of organic functional groups. *Curr Drug Metab* 6:161-225.

Lambert SM, Langley DR, Garnett JA, Angell R, Hedgethorpe K, Meanwell NA, Matthews SJ (2014) The crystal structure of NS5A domain 1 from genotype 1a reveals new clues to the mechanism of action for dimeric HCV inhibitors. *Protein Sci* 23:723-734.

Lavanchy D (2009) The global burden of hepatitis C. *Liver Int* 29(s1):74-81.

Lesburg CA, Cable MB, Ferrari E, Hong Z, Mannarino AF, and Weber PC (1999) Crystal structure of the RNA-dependent RNA polymerase from hepatitis C virus reveals a fully encircled active site. *Nature Structural Biology* 6:937-943.

Lohmann V, Körner F, Koch J-O, Herian U, Theilmann L, Bartenschlager R (1999) Replication of subgenomic hepatitis C virus RNAs in a hepatoma cell line. *Science* 285:110-113.

Lok AS, Gardiner DF, Lawitz E, Martorell C, Everson GT, Ghalib R, Reindollar R, Rustgi V, McPhee F, Wind-Rotolo M, Persson A, Zhu K, Dimitrova DI, Eley T, Guo

DMD # 68866

T, Grasela DM, Pasquinelli C (2012) Preliminary study of two antiviral agents for hepatitis C genotype 1. *New Engl J Med* 366:216-224.

Lopez OD, Nguyen VN, St Laurent DR, Belema M, Serrano-Wu MH, Goodrich JT, Yang F, Qiu Y, Ripka AS, Nower PT, Valera L, Liu M, O'Boyle II DR, Sun J-H, Fridell RA, Lemm JA, Gao M, Good AC, Meanwell NA, Snyder LB. (2013) HCV NS5A replication complex inhibitors. Part 3: Discovery of potent analogues with distinct core topologies. *Bioorg Med Chem Lett* 23:779-784.

Love RA, Brodsky O, Hickey MJ, Wells PA, Cronin CN (2009) Crystal structure of a novel dimeric form of NS5A domain I protein from hepatitis C virus. *J Virol* 83:4395-4403.

McPhee F, Sheaffer AK, Friberg J, Hernandez D, Falk P, Zhai G, Levine S, Chaniewski S, Yu F, Barry D, Chen C, Lee MS, Mosure K, Sun LQ, Sinz M, Meanwell NA, Colonna RJ, Knipe J, Scola P (2012) Preclinical profile and characterization of the hepatitis C virus NS3 protease inhibitor asunaprevir (BMS-650032). *Antimicrob Agents Chemother* 56:5387-5396.

Nelson DR, Cooper JN, Lalezari JP, Lawitz E, Pockros PJ, Gitlin N, Freilich BF, Younes ZH, Harlan W, Ghalib R, Oguchi G, Thuluvanth PJ, Ortiz-Lasanta G, Rabinovitz M, Bernstein D, Bennett M, Hawkins T, Ravendhran N, Sheikh AM, Varunok P, Kowdley KV, Hennicken D, MCPhee F, Rana K, Hughes EA, ALLY-3 Study Team (2015) All-oral 12-week treatment with daclatasvir plus sofosbuvir in patients with hepatitis C virus genotype 3 infection: ALLY-3 phase III study. *Hepatology* 61:1127-1135.

Penin F, Brass V, Appel N, Ramboarina S, Montserret R, Ficheux D, Blum HE, Bartenschlager R, Moradpour D (2004) Structure and function of the membrane anchor domain of hepatitis C virus nonstructural protein 5A. *J Biol Chem* 279:40835-40843.

Rodriguez-Torres M, Lawitz E, Kowdley KV, Nelson DR, Dejesus E, McHutchison JG, Cornpropst MT, Mader M, Albanis E, Jiang D, Hebner CM, Symonds WT, Berrey MM, Lalezari J (2013) Sofosbuvir (GS-7977) plus peginterferon/ribavirin in treatment-

DMD # 68866

naïve patients with HCV genotype 1: a randomized, 28-day, dose-ranging trial. *J Hepatol* 58:663-668.

Romine JL, St. Laurent, DR, Leet JE, Martin SW, Serrano-Wu MH, Yang, F, Gao M, O'Boyle II D R, Lemm, J. A, Sun J-H, Nower PT, Huang X, Deshpande, MS, Meanwell NA, Snyder LB (2011) Inhibitors of HCV NS5A: From iminothiazolidinones to symmetrical stilbenes. *ACS Med Chem Lett* 2:224-229.

Schabbert S, Pierschbacher MD, Mattern R-H, Goodman M (2002) Incorporation of (2S,3S) and (2S,3R)  $\beta$ -methyl aspartic acid into RGD-containing peptides. *Bioorg Med Chem* 10, 3331-3337.

Sofia MJ, Bao D, Chang W, Du J, Nagarathnam D, Rachakonda S, Reddy PG, Ross BS, Wang P, Zhang HR, Bansal S, Espiritu C, Keilman M, Lam AM, Steuer HM, Niu C, Otto MJ, Furman PA (2010) Discovery of a  $\beta$ -D-2'-deoxy-2'- $\alpha$ -fluoro-2'- $\beta$ -C-methyluridine nucleotide prodrug (PSI-7977) for the treatment of hepatitis C virus. *J Med Chem* 53:7202-7218.

St Laurent DR, Belema M, Gao M, Goodrich J, Kakarla R, Knipe JO, Lemm JA, Liu M, Lopez OD, Nguyen VN, Nower PT, O'Boyle II D, Qiu Y, Romine JL, Serrano-Wu MH, Sun J-H, Valera L, Yang F, Yang X, Meanwell NA, Snyder LB (2012) HCV NS5A replication complex inhibitors. Part 2: Investigation of stilbene prolinamides. *Bioorg Med Chem Lett* 22:6063-6066.

St. Laurent DR, Serrano-Wu MH, Belema M, Ding M, Fang H, Gao M, Goodrich JT, Krause RG, Lemm JA, Liu M, Lopez O, Nguyen VN, Nower PT, O'Boyle II DR, Pearce BC, Romine JL, Valera L, Sun J-H, Wang Y-K, Yang F, Yang X, Meanwell NA, Snyder LB. (2013) HCV NS5A replication complex inhibitors. Part 4: Optimization for genotype 1a replicon inhibitory activity. *J Med Chem* 57:1976-1994.

Seglen PO (1976) Preparation of isolated rat liver cells. *Methods Cell Biol* 13:29-83.

DMD # 68866

Sun J-H, O'Boyle II DR, Fridell RA, Langley DR, Wang C, Roberts SB, Nower P, Johnson BM, Moulin F, Nophsker MJ, Wang Y-K, Liu M, Rigat K, Tu Y, Hewawasam P, Kadow J, Meanwell NA, Cockett M, Lemm JA, Kramer M, Belema M, Gao M (2015) Resensitizing daclatasvir-resistant hepatitis C variants by allosteric modulation of NS5A. *Nature* doi:10.1038/nature15711

Tellinghuisen TL, Marcotrigiano J, Gorbalenya AE, Rice CM (2004) The NS5A protein of hepatitis C virus is a zinc metalloprotein. *J Biol Chem* 279:48576-48587.

Tellinghuisen TL, Marcotrigiano J, Rice CM (2005) Structure of the zinc-binding domain of an essential component of the hepatitis C virus replicase. *Nature* 435:374-379.

Wyles DL, Ruane PJ, Sulkowski MS, Dieterich D, Luetkemeyer A, Morgan TR, Sherman KE, Dretler R, Fishbein D, Gathe Jr JC, Henn S, Hiney C, McDonald C, Mills A, Overton ET, Ramgopal M, Rashbaum B, Ray G, Scarsella A, Yozviak J, McPhee F, Liu Z, Hughes E, Yin PD, Noviello S, Ackerman P, ALLY-2 Investigators (2015) Daclatasvir plus sofosbuvir for HCV in patients coinfecting with HIV-1. *N Engl J Med* 373:714-725.

DMD # 68866

## Legends

Fig. 1. Structure of daclatasvir (**1**). Atom numbers are for illustrative purposes and do not conform to International Union of Pure and Applied Chemistry nomenclature.  $^{14}\text{C}$  was incorporated at positions C4 and C29 during the synthesis of [ $^{14}\text{C}$ ]-**1**, and this material was used for most experiments. Alternatively,  $^3\text{H}$  was incorporated at positions C5 and C33 during the synthesis of [ $^3\text{H}$ ]-**1**, and this material was used for the covalent binding study.

Fig. 2. Positive-ion electrospray product-ion MS/MS spectra of **1**, **2**, **3**, and **4**, with annotated structures describing the interpretation of fragmentation patterns. Spectra were acquired using an ion trap mass spectrometer employing collision-induced dissociation and a normalized collision energy of 40%. A) Compound **1** underwent neutral loss of the valine methyl carbamate moiety yielding a product ion of  $m/z$  565. Additional fragmentation of this ion by an equivalent neutral loss on the opposite side of the ion, and by cleavage of the C31/C38 bond, yielded minor downstream product ions of  $m/z$  391 and 339, respectively. These ions were detected during MS/MS of multiple metabolites as listed in Table 2. B) The structures of **2** were elucidated based on these MS/MS spectra and by comparison to synthetic standards. C) The structure of **3** illustrated above is consistent with the MS/MS spectrum shown but required additional analysis by NMR for a complete structure determination to be made. The intense pair of MS/MS peaks of  $m/z$  580 and 581 was also observed in the MS/MS spectra of bis-oxidation products of **1** (e.g. **14**, **19**, **25**) and came to be interpreted as a mark of pyrrolidine rearrangement. D) The

DMD # 68866

structure of **4** were elucidated based on these MS/MS spectra and by comparison to synthetic standards.

Fig. 3. Pathways proposed for the biotransformation of daclatasvir (**1**). The main metabolite **3**, was formed by *N*-dealkylation followed by intramolecular nucleophilic attack of the imidazole *N1* on the nascent propanal-3-yl group. The remaining metabolites were generally minor products in nonclinical species. The structures of **1 – 4** and **7 – 8** were confirmed by comparison to reference standards, and the structures of **5, 9 – 23**, and **25 – 26** were proposed based on positive-ion MS/MS spectra. A diastereomer of **7** were synthesized but could not be matched against any observed metabolites of **1**.

Fig. 4. <sup>1</sup>H NMR spectra of daclatasvir (**1**) (top), the isolated metabolite **3** (middle) and the synthetic standard of **3** (bottom) in DMSO-*d*<sub>6</sub>

Fig. 5. <sup>1</sup>H-<sup>13</sup>C HSQC spectra of the isolated metabolite **3** (top) and the synthetic standard of **3** (bottom)

Fig. 6. Diagnostic through-bond and through-space correlations of **3** observed in 2D NMR spectra. Atoms and atom numbers are shown in bold type, and chemical shifts are shown in standard type. A. <sup>1</sup>H-<sup>1</sup>H through-bond correlations (COSY, TOCSY). B. <sup>1</sup>H-<sup>1</sup>H spatial interactions (TROESY). C. <sup>1</sup>H-<sup>13</sup>C long-range correlations (HMBC).

DMD # 68866

TABLE 1

*Methods used to measure the inhibition of P450 enzymes by daclatasvir in human liver microsomes*

Reaction components, conditions, and mass spectrometry settings used in the analysis of probe metabolites were developed separately for each assay as tabulated below.

CYP Enzyme	1A2	2B6	2C8	2C9	2C19	2D6	3A4
Probe	tacrine	bupropion	amodiaquine	diclofenac	S-mephenytoin	dextromethorphan	testosterone
Substrate						phan	
Concentration (μM)	3	100	2	5	50	10	75
HLM Protein Concentration (mg/mL)	0.15	0.1	0.05	0.15	0.25	0.15	0.15
Metabolite	1'-hydroxytacrine	hydroxybupropion	desethylamodiaquine	4'-hydroxydiclofenac	4'-hydroxymephenytoin	dextrorphan	6β-hydroxytestosterone
Internal Standard	Bucetin	[ <sup>2</sup> H <sub>6</sub> ]-hydroxybupropion	[ <sup>2</sup> H <sub>5</sub> ]-desethylamodiaquine	[ <sup>13</sup> C <sub>6</sub> ]-4'-hydroxydiclofenac	[ <sup>2</sup> H <sub>3</sub> ]-4'-hydroxymephenytoin	[ <sup>2</sup> H <sub>3</sub> ]-dextrorphan	[ <sup>2</sup> H <sub>3</sub> ]-6β-hydroxytestosterone
Internal Standard Concentration (μM)	0.2	0.2	0.075	0.2	0.1	0.2	1
Incubation Time (min)	15	15	10	10	45	7	5
MS Mode	Positive ESI	Positive APCI	Positive ESI	Positive ESI	Positive APCI	Positive ESI	Positive ESI
Metabolite Transition	215.2 → 182.2	256.1 → 184.2	328.2 → 282.8	312.0 → 230.8	235.1 → 133.2	258.2 → 156.8	305.1 → 230.1
Internal Standard Transition	224.2 → 108.1	262.1 → 184.2	331.2 → 282.8	318.0 → 236.8	238.1 → 133.2	261.2 → 156.8	308.1 → 272.2

DMD # 68866

Declustering Potential	45 V	45 V	55 V	50 V	50 V	90 V	80 V
Collision Voltage	45 V	21 V	26 V	28 V	25 V	55 V	21 V
Dwell Time	80 ms	80ms	250 ms				

---

DMD # 68866

TABLE 2

*Liquid chromatography—tandem mass spectrometric data of metabolites of daclatasvir  
that were detected in vitro and in animals*

Analytes were separated using a 75-min reversed-phase HPLC gradient as described in the Materials and Methods section. Precursor ions tabulated correspond to the monoisotopic masses of the unlabeled ( $^{12}\text{C}$ ) compound. A normalized collision energy of 40% was used to generate the product ions listed.

Compound	Retention Time (min)	Precursor Ion $[\text{M}+\text{H}]^+$	Product Ions $m/z$
1	56.2	739	339, 391, 513, 565, 582, 707
2	34.7	755	339, 391, 513, 529, 565, 581, 582, 608, 737
3	41.2	755	407, 513, 563, 580, 581, 737
4	24.8	681	339, 391, 455, 507, 513, 565, 582, 649
5	22.1	697	355, 407, 549, 580, 581, 679
6	51.9	755	513, 529, 563, 581, 598, 723, 737
7	43.8	755	407, 529, 549, 581, 582, 598, 723
8	17.7	519	249, 301, 443, 475
9	53.1	755	303, 355, 529
10	38.3	755	507, 529, 563, 598, 723
11	30.8	771	299, 422, 473, 596, 614, 753
12	28.6	771	371, 379, 423, 553, 597
13	54.8	771	544, 596, 614
14	26.4	771	355, 407, 563, 580, 581, 597
15	18.0	598	372, 424, 441, 566
16	19.8	803	393, 411, 437, 455, 585, 629, 646
17	22.8	787	379, 423, 553, 597
18	39.4	757	409, 551, 583

DMD # 68866

---

<b>19</b>	27.2	771	355, 407, 580, 581, 753
<b>20</b>	57.2	769	438, 543, 595, 612, 737, 751
<b>21</b>	58.3	769	438, 543, 595, 612, 737, 751
<b>22</b>	26.0	521 [M+H <sub>2</sub> O+H] <sup>+</sup>	277, 295, 329, 347, 471, 489, 503
<b>23</b>	22.3	901	582, 681, 725
<b>25</b>	31.4	771	407, 563, 580, 581, 713
<b>26</b>	22.4	491	265, 317, 334, 459

---

DMD # 68866

TABLE 3

*Relative abundances of [<sup>14</sup>C]-daclatasvir and its metabolites following incubations in vitro*

[<sup>14</sup>C]-Daclatasvir (**1**) was incubated with liver microsomes (M) supplemented with GSH (5 mM) and NADPH (1 mM), liver S9 (S) supplemented with NADPH (1 mM), arochlor-induced rat liver S9 (ARS) supplemented with NADPH (1 mM), and hepatocytes (H).

Results are tabulated here. Abundances are based on the intensity of radioactivity in fractions containing metabolites, calculated relative to the total amount of radioactivity in each sample. The sum of radioactivity in each column is less than the total radioactivity, reflecting the presence of minor metabolites that were not identified. Other abbreviations:

- = not detected, ms = detected by mass spectrometry only.

Compound	Mouse			Rat			Dog			Monkey			Human		
	M	S	H	M	ARS	H	M	S	H	M	S	H	M	S	H
<b>1</b>	84	83	83	82	74	78	81	87	82	73	73	58	78	80	89
<b>2</b>	-	-	-	-	-	ms	-	-	ms	-	-	ms	4.2	2.4	ms
<b>3</b>	2.4	1.4	1.6	8.3	6.3	11	1.9	2.0	2.1	18	15	23	11	9.2	6.3
<b>4</b>	4.0	3.8	6.4	ms	1.0	2.2	4.0	2.8	10	1.5	1.0	7.4	0.3	0.4	ms
<b>5</b>	ms	ms	ms	ms	-	ms	ms	ms	ms	ms	ms	2.9	-	-	-
<b>7</b>	ms	-	0.7	-	-	ms	-	-	ms	-	-	-	ms	ms	ms
<b>8</b>	ms	0.4	ms	ms	1.4	ms	-	-	ms	0.3	ms	ms	0.3	ms	ms
<b>10</b>	ms	ms	ms	-	-	ms	-	-	-	-	-	ms	-	-	ms
<b>11</b>	ms	ms	-	ms	0.9	-	ms	ms	-	-	-	-	0.2	-	-
<b>12</b>	-	-	-	-	-	-	-	-	-	-	-	2.7	-	-	-
<b>15</b>	-	-	-	-	-	-	-	-	-	-	-	ms	-	-	-

DMD # 68866

<b>26</b>	ms	0.3	ms	ms	3.2	ms	ms	ms	0.4	0.3	0.2	ms	ms	ms	0.3
<b>Sum</b>	91	89	92	90	86	91	87	91	95	93	89	94	94	92	96

DMD # 68866

TABLE 4

*Rates of covalent binding to protein across species*

[<sup>3</sup>H]-Daclatasvir ([<sup>3</sup>H]-**1**; 10 μM) was incubated in triplicate with pooled dog, human, rat, or monkey liver microsomes (1 mg protein/mL) for 1 h at 37 °C. Incubations were performed both in the presence and absence of glutathione (5 mM). [<sup>3</sup>H]-Imipramine (10 μM) was also incubated under identical conditions as a positive control.

	without NADPH	with NADPH	with NADPH and glutathione
<hr/>			
[ <sup>3</sup> H]-daclatasvir ( <b>1</b> )			
human	15.8 ± 5.0	55.2 ± 8.1	40.9 ± 7.2
rat	13.0 ± 0.1	57.6 ± 10.7	22.4 ± 3.0
monkey	19.6 ± 2.3	67.8 ± 21.0	25.2 ± 5.8
[ <sup>3</sup> H]-imipramine			
human	16.5 ± 1.9	218.9 ± 45.6	17.1 ± 9.6
<hr/>			

DMD # 68866

TABLE 5

*Distribution of radioactivity in plasma*

[<sup>14</sup>C]-Daclatasvir ([<sup>14</sup>C]-1) was administered p.o. as a single dose to intact animals (mice, rats, monkeys) and to BDC animals (dogs), and plasma was collected at selected time points over 8 h. Samples were processed as described in the Materials and Methods section and analyzed by LC-MS/MS with fraction collection and offline scintillation counting. Data is expressed as a percentage of the radioactivity in each sample. The sum of radioactivity reported in some columns is less than the total radioactivity, reflecting the presence of minor metabolites that were not identified Abbreviations: - = not detected, ms = detected by mass spectrometry only.

	Mouse		Rat			BDC Dog			Monkey		
	1 h	4 h	1 h	2 h	4 h	1.5 h	4 h	8 h	1 h	4 h	8 h
<b>1</b>	89.8	74.6	84.6	85.2	88.2	87.5	92.4	93.9	78.2	74.2	85.6
<b>3</b>	1.6	4.0	2.9	2.8	2.6	ms	ms	ms	21.8	17.8	14.4
<b>4</b>	3.2	2.1	2.0	3.0	1.9	ms	2.3	2.0	-	-	-
<b>5</b>	1.5 <sup>a</sup>	3.0 <sup>a</sup>	-	-	-	ms	1.2 <sup>a</sup>	0.6 <sup>a</sup>	-	-	-
<b>26</b>			4.5	4.0	3.5	ms			-	-	-
<b>7</b>	2.8	6.7	-	-	-	-	-	-	-	-	-
<b>8</b>	-	-	1.5	2.0	1.5	-	-	-	-	-	-
<b>9</b>	ms	1.5	0.3	0.7	0.7	2.9	ms	ms	-	-	-
<b>10</b>	ms	2.4	-	-	-	-	-	-	-	-	-
<b>12</b>	-	-	-	-	-	-	-	-	ms	2.1	ms
<b>Sum</b>	98.9	94.3	95.8	97.7	98.4	90.4	95.9	96.5	100.0	94.1	100.0

DMD # 68866

- a. Compounds **5** and **26** coeluted during HPLC. Entries represent the sum of radioactivity attributed to these two metabolites.

DMD # 68866

TABLE 6

*Distribution of radioactivity in bile and feces*

[<sup>14</sup>C]-Daclatasvir ([<sup>14</sup>C]-1) was administered p.o. as a single dose to intact animals (mice, rats, monkeys) and to BDC animals (dogs, monkeys, rats), and bile and feces were collected over periods of 2 – 7 days. Samples were processed as described in the Materials and Methods section and analyzed by LC-MS/MS with fraction collection and offline scintillation counting. Data is expressed as a percentage of the radioactivity administered. The sum of radioactivity listed in the bottom row does not account for minor metabolites unidentified or drug-related materials recovered in urine, cage rinse and wipe, or carcass. Abbreviations: - = not detected, ms = detected by mass spectrometry only.

	Feces				Bile		
	Mouse (0-168 h)	Rat (0- 168 h)	BDC Dog (0-72 h)	Monkey (0-168 h)	BDC Rat (0-48 h)	BDC Dog (0-72 h)	BDC Monkey (0-72 h)
<b>1</b>	34.0	24.5	16.6	32.3	11.5	12.5	1.4
<b>2</b>	-	-	-	-	0.7	0.1	ms
<b>3</b>	1.1	2.0	2.0	16.8	10.1	2.9	7.2
<b>4</b>	5.9	3.7	3.1	0.9	2.2	2.6	0.2
<b>5</b>	-	-	1.1	-	2.5 <sup>a</sup>	0.6	0.4 <sup>a</sup>
<b>26</b>	-	-	-	-			
<b>7</b>	-	-	-	-	2.5	-	0.1
<b>8</b>	7.3	9.4	1.6	1.0	1.6	-	0.1
<b>9</b>	1.0	-	-	0.6	0.5	-	0.03

DMD # 68866

<b>10</b>	-	-	-	-	0.5	-	ms
<b>11</b>	3.1	4.9	0.2	1.0	-	-	-
<b>12</b>	-	-	-	1.9	0.4	0.1	1.6
<b>13</b>	-	2.8	-	-	-	-	-
<b>14</b>	-	-	-	-	-	-	0.2
<b>15</b>	-	-	-	-	-	-	0.3
<b>16</b>	-	-	-	-	-	-	0.2
<b>17</b>	-	-	-	-	-	-	0.4
<b>18</b>	-	-	-	2.2	-	-	0.2
<b>19</b>	-	-	-	-	-	-	0.4
<b>20</b>	-	-	0.5	1.0	0.7	-	0.1
<b>21</b>	-	-	-	0.6	0.1	-	0.1
<b>22</b>	-	4.1	-	-	-	-	-
<b>23</b>	-	-	-	-	-	1.2	-
<b>25</b>	-	-	-	-	-	-	0.2
<b>Sum</b>	52.4	51.4	25.1	58.3	30.8	20	12.73

- a. Compounds **5** and **25** coeluted during HPLC. Entries represent the sum of radioactivity attributed to these two metabolites.

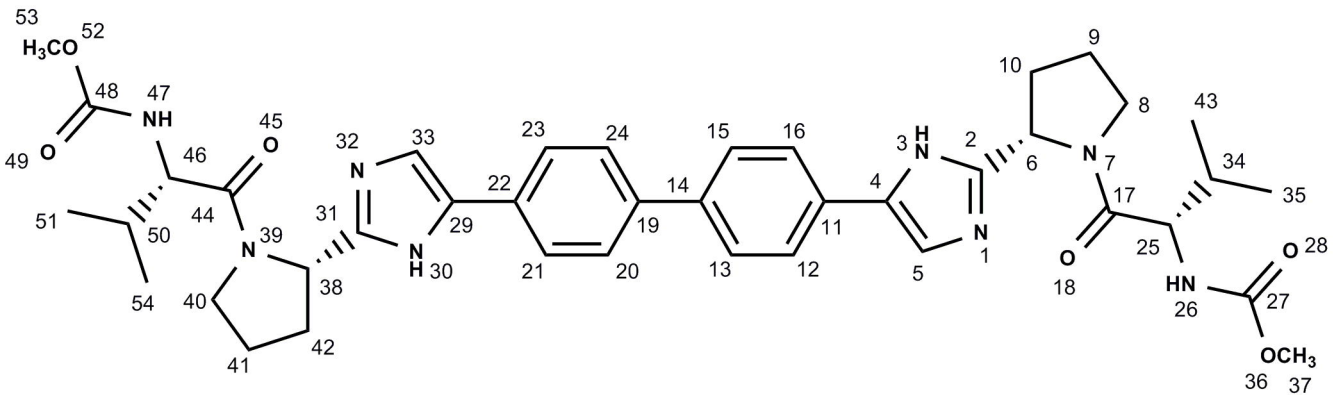
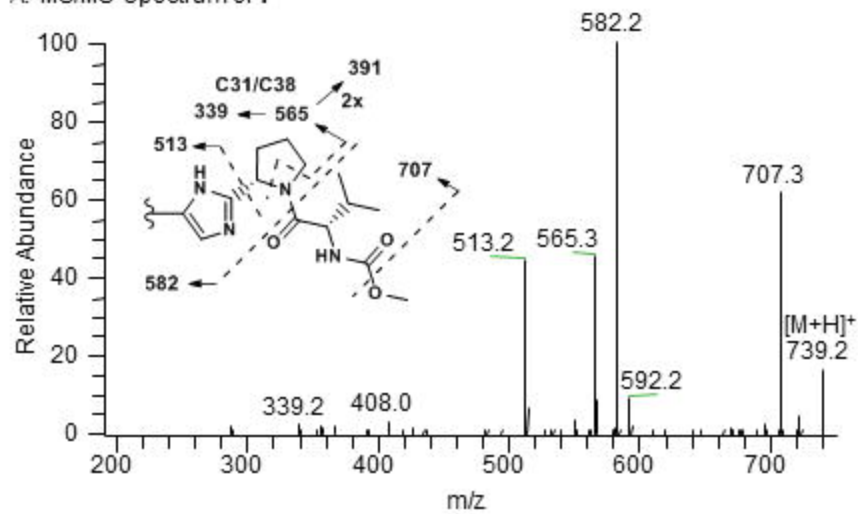


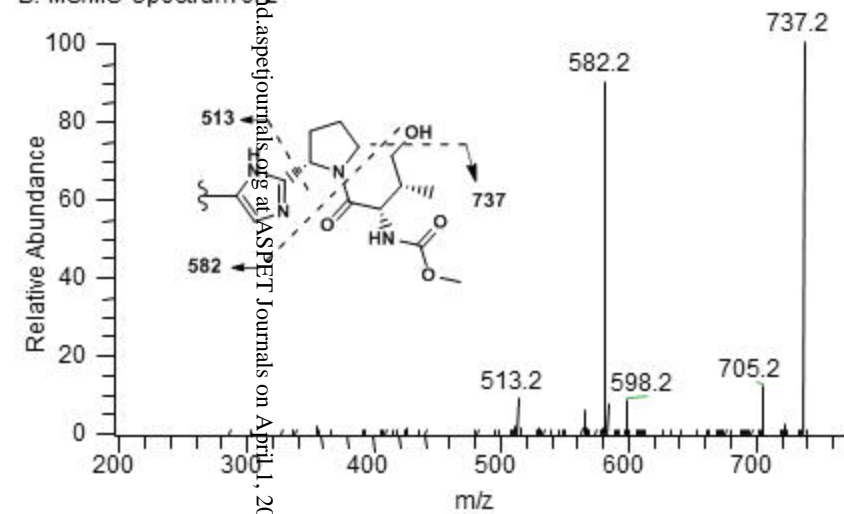
Fig. 1



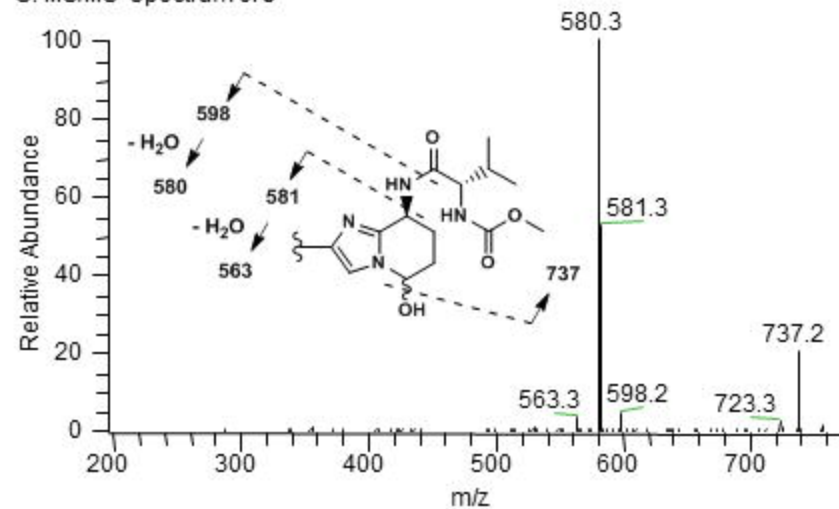
A: MS/MS spectrum of **1**



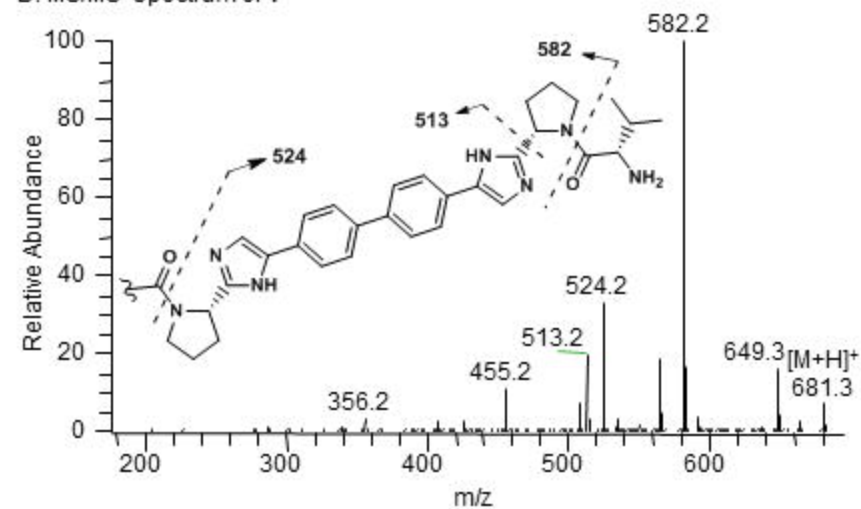
B: MS/MS spectrum of **2**



C: MS/MS spectrum of **3**



D: MS/MS spectrum of **4**



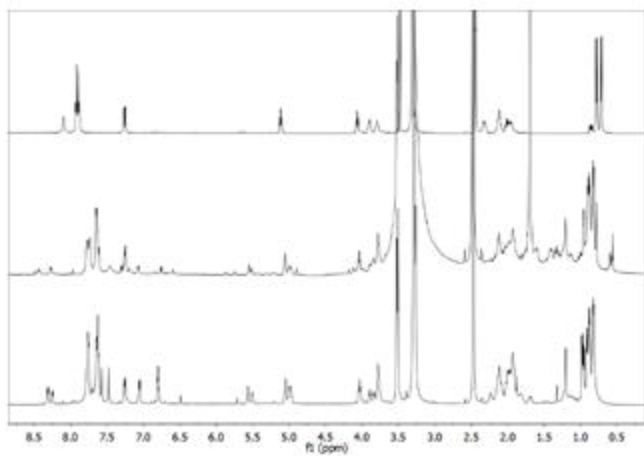


Fig. 4

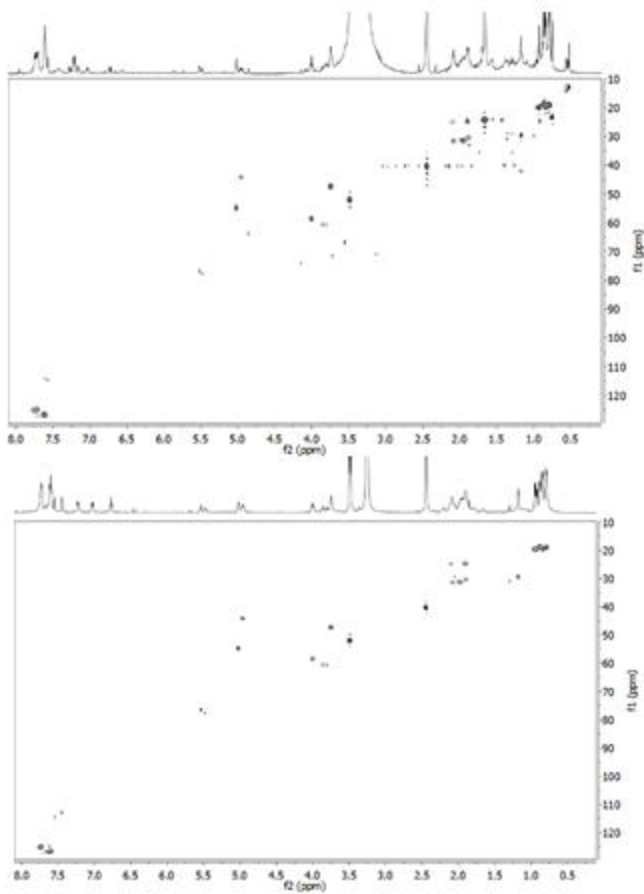


Fig. 5

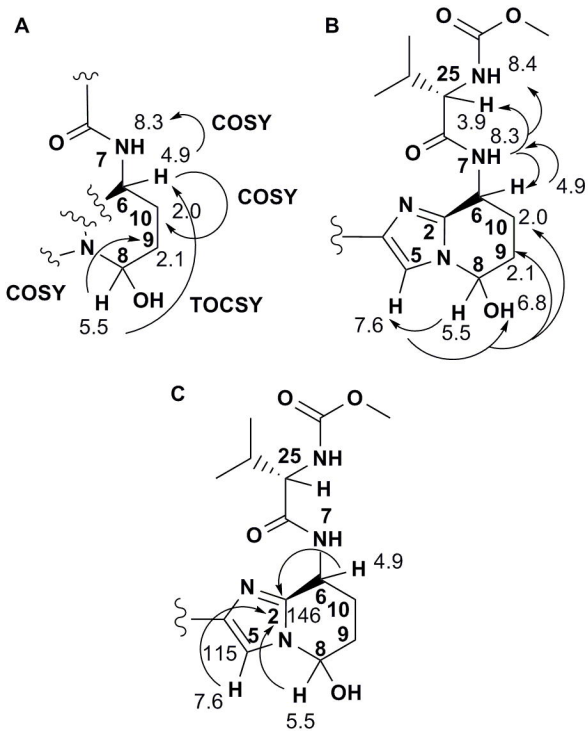


Fig. 6